TGIF: Topological Gap In-Fill for Vascular Networks
A Generative Physiological Modeling Approach

Matthias Schneider[1,2], Sven Hirsch[1], Bruno Weber[2], Gábor Székely[1], and Bjoern H. Menze[1,3]

[1] Computer Vision Laboratory, ETH Zurich, Switzerland
[2] Institute of Pharmacology and Toxicology, University of Zurich, Switzerland
[3] Institute for Advanced Study and Department of Computer Science, TU Munich, Germany

Abstract. This paper describes a new approach for the reconstruction of complete 3-D arterial trees from partially incomplete image data. We utilize a physiologically motivated simulation framework to iteratively generate artificial, yet physiologically meaningful, vasculatures for the correction of vascular connectivity. The generative approach is guided by a simplified angiogenesis model while at the same time topological and morphological evidence extracted from the image data is considered to form functionally adequate tree models. We evaluate the effectiveness of our method on four synthetic datasets using different metrics to assess topological and functional differences. Our experiments show that the proposed generative approach is superior to state-of-the-art approaches that only consider topology for vessel reconstruction and performs consistently well across different problem sizes and topologies.

Keywords: vascular reconstruction, vascular connectivity, angiogenesis

1 Introduction

Vascular image analysis plays a crucial role in many research areas and has various applications. In neuroscience, for instance, gaining further insight into the topological and morphological properties of the cortical microvasculature is fundamental to a better understanding of the neurovascular coupling and regulation in neurodegenerative diseases such as Alzheimer's [1]. Advances in high-resolution imaging modalities, e.g., synchrotron radiation micro-CT, have greatly facilitated the acquisition of highly detailed image data of complex vascular systems across different scales down to the capillary level [8]. However, the analysis and reconstruction of complete vascular networks is still an open problem despite extensive ongoing research in vascular image analysis. Most of the research addresses the problem of *vessel detection* and *segmentation* [4] while mostly neglecting *vascular connectivity* [9]. Incomplete connectivity dramatically complicates or even precludes the analysis of hemodynamic and metabolic properties [1, 8]. Topological defects are commonly caused by limitations of the reconstruction methodology (e.g. invalid model assumptions) or problems related to image acquisition (image noise, artifacts) and sample preparation (insufficient dye filling, air bubbles, clotting).

There is only very little previous work on reconstruction and correction of vessel connectivity [4, 9]. A popular principle is the extraction of a minimum spanning tree (MST) w.r.t. different distance metrics based on Euclidean distance or physiological principles [2, 4]. Risser et al. [10] proposed a gap filling approach based on tensor

voting. The authors use local directional and morphological information to define a tensor field supporting likely vessel pathways to be tracked to fill gaps. More recently, Kaufhold et al. [3] presented a learning-based algorithm to recover missing connectivity by threshold relaxation relying on last traces of information in the image data that have been missed before. Though in case of total signal loss at a gap (e.g. caused by incomplete filling with dye), their method is no longer applicable.

The slightly different and more fundamental problem of synthetic formation of functionally adequate vascular networks has attracted considerable attention in the field of computational physiology [5, 12, 13]. Here, physiological principles are applied to generate synthetic vascular models that satisfy prescribed physiological conditions.

In this work, we combine different key ideas of both aforementioned problem classes to reconstruct consistent 3-D arterial trees from partially incomplete image data. We utilize artificially generated, yet physiologically plausible, vascular structures for the correction of vascular connectivity. To this end, we adapt a simulation framework based on a simplified angiogenesis model to iteratively complete the defective vasculature taking into account the topological and morphological evidence extracted from the image data. The primary objective of this work is first and foremost the reconstruction of a physiologically meaningful vasculature rather than the recovery of the exact topology.

2 Methods

Generating new vascular structures. The proposed approach for topological gap in-fill (TGIF) is primarily based on our generative model for the construction of synthetic 3-D arterial tree models as introduced in [12]: The physiologically motivated method combines a simplified model for sprouting angiogenesis stimulated by a growth factor with structural remodeling and degeneration in response to morphological and metabolic stimuli to iteratively generate an arterial tree model until the (prescribed) metabolic demand of the embedding tissue is met, i.e., no hypoxic regions left. The vascular system is modeled as a set of binary trees where each vessel branch is approximated by a sequence of edges (vessel segments) each representing a cylindrical tube of fixed length and radius. Additional morphological constraints are enforced at construction time with regard to the morphometrical configuration at bifurcations, i.e., relationship of radii (Murray's law) and optimal bifurcation angles derived from Murray's minimum work principle (MWP). The iterative growth proceeds in four steps [12]:

(S1) Angiogenesis model: reaction-diffusion process to estimate tissue perfusion and oxygenation as well as the corresponding concentration map of vascular endothelial growth factors (VEGFs) emitted by hypoxic-ischemic cells.
(S2) Vascular growth forming new sprouts in chemotactic response to VEGF.
(S3) Structural remodeling and degeneration of redundant vascular structures.
(S4) Repeat steps (S1)–(S3) until prescribed tissue metabolism is met.

To apply this concept [12], we identify feeding vessels (root nodes) entering the image volume and isolated vascular components with no connection to any root. As these unrooted parts are lacking blood supply (stagnant hypoxia), they do not contribute to the perfusion of the surrounding tissue estimated in step (S1). The resulting hypoxic areas lead to locally increased VEGF secretion attracting new sprouts. Thus, step (S2) iteratively grows new sprouts originating from rooted (perfused) segments following the

local VEGF gradient (constant step length δ), and the sprouting tip is connected to an unrooted segment when it gets closer than $4\,\mu$m. Still, due to the sparse vascularization of 3-D tissues ($\approx 2\,\%$ vascular volume fraction [8]), a sprouting tip would rarely hit another unrooted vessel if purely driven by angiogenesis [13]. Thus, we propose to amend the generative model by an "attractor" to enforce such connections between vessel segments if supported by the topology and morphology, which we discuss next.

Connecting Unrooted Segments. We allow rooted sprouts to link with nearby unrooted vascular structures in step (S2). Similar to [13], we define the set of potential connection candidates at a sprouting tip as unrooted vessel segments lying within a spherical-cone-shaped sector along the sprout direction (maximum distance $R_{\text{max}} = 100\,\mu$m, angular deviation $\theta_{\text{max}} = 60°$ [13, Tbl. 1]). To find the optimal connection candidate for a sprouting node v_s with proximate connection candidates $v_c \in \mathcal{V}_c$, we first rank the connecting edges $e = (v_s, v_c)$ w.r.t. the heuristic cost function (HCF) proposed by Reichold [8] considering directional and spatial information. This parametric model favors short over long infills, but also a minimal bending angle of the new connection:

$$C_{\text{HCF}}(e) = \lambda_{\text{d}} \cdot \frac{l(e)}{d_{\text{max}}} + (1 - \lambda_{\text{d}}) \cdot \left[1 - \exp\left(-\frac{\alpha}{\alpha_0}\right)\right] \left[1 - \operatorname{erf}\left(\frac{l(e)}{d_0}\right)\right] , \quad (1)$$

where $l(e) \leq d_{\text{max}}$ denotes the edge length, and $\lambda_{\text{d}} \in [0, 1]$ is a weighting factor to balance the distance-based and angle-based term. The bending angle α is defined as the sum of the bending angles relative to the vessel direction at v_s and v_c, respectively (see supplementary material for illustrations of C_{HCF}). The parameter d_0 defines the maximum distance beyond which the influence of α is negligible. The factor α_0 is used to shape the angle-dependent term. As the ranking of the candidate edges w.r.t. C_{HCF} is not symmetric, i.e., the top-ranked edge (v_s, v_t) of v_s can be ranked very low at v_t, we apply a k-reciprocal neighborhood search [7]: From the top k_{rNN} ranked candidate edges of v_s, we pick the highest ranked edge $\hat{e} = (v_s, \hat{v}_t)$ for which $\check{e} = (\hat{v}_t, v_s)$ is among the k_{rNN} highest ranked edges of $\hat{v}_t$. If there is no such "k_{rNN}-optimal" edge $\hat{e}$, we follow the homing mechanism proposed by Secomb et al. [13, Eq. 10–14] that makes sprouting tips susceptible to nearby vessel segments, i.e., the growth direction of the evolving sprout is computed as the weighted sum over the set of potential connection candidates as defined above (sensitivity $k_V = 10$ [13, Tbl. 1])). Finally, if the sprouting tip does not sense any proximate vessel segments, i.e., empty set of connection candidates, we fall back to the VEGF-based strategy in step (S2) to determine the growth direction.

Remodeling. Adding new vascular connections modifies the network topology and – under consideration of global geometrical constraints, such as continuity of radii along connections and radii at bifurcations following Murray's law – we have to update the vessel diameters in step (S3) to match the new conditions. To this end, we adjust the diameters of newly generated vessels (*synthetic* nodes) and maintain estimated vessel radii at *static* nodes with strong evidence in the image data.

Every synthetic subtree generated at an infill location has a well-defined static root node n_r at the proximal transition from static to synthetic data. Also, each terminal node at the distal end of the subtree is either (1) non-static, i.e., newly generated sprouting tip not yet linked with a connection candidate, or (2) static, i.e., transition from synthetic to static data with prescribed radius. We iteratively remodel the subtree as follows:

(R1) Prescribe vessel radius at static terminal nodes according to image evidence.
(R2) Propagate radii from all subtree terminals to root n_r according to Murray's law [12].

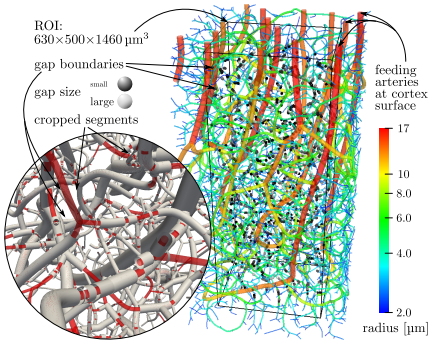

Fig. 1: Synthetic vascular tree model with artificial gaps ($\mathcal{B}_2$, $\gamma_{\text{crop}} = 32\,‰$).

Method	Parameter	Value/Range		Text/Reference
MWP	λ_{MWP}	$\{0.0, 0.1, 0.2, 0.3, 0.4, 0.5\}$		[2, Eq. 13]
TV	L	see d_{max}		[10, Eq. 6]
	θ	$\{15°, 30°, 45°, 60°\}$		[10, Eq. 6]
	l_{max}	$\{0.5, 1.0, 1.5, 2.0\} \times s_{\text{gap}}$	[$\mathcal{B}_1$]	[10, Sec. III.K.4]
		$\{12, 48, 96, 144\}$[µm]	[$\mathcal{B}_2$]	
	s_{min}	$\{10^{-4}, 10^{-2}, 10^{-1}, 0.5\}$		[10, Sec. III.K.4]
HCF	d_{max}	$\{0.5, 0.75, 1.0, 1.5, 2.0\} \times s_{\text{gap}}$	[$\mathcal{B}_1$]	Eq. (1)
		$\{12, 24, 48, 96\}$[µm]	[$\mathcal{B}_2$]	
	λ_{d}	$\{\underline{0.4}, 0.5, 0.6, 0.7\}$		
	α_0	$\{\underline{100}°, 120°, 140°, 160°\}\,/\,\log(2)$		
	d_0	$\{0.5, 1.0, 2.0, \underline{4.0}\} \times d_{\text{max}}$		
	k_{rNN}	$\{\underline{1}, 2, 4, 6\}$		
TGIF	λ_g	$\{1, 2, 4, 8\}$		[12, Eq. 12]
	δ	$\{8, 16, 32, 64\}$[µm]		
	ξ	$\{1.00, 1.05, 1.10, 1.15)$		(R3)

Table 1: Examined parameter ranges for different reconnection approaches. Default HCF parameters used for TGIF are underlined.

(R3) STOP if for updated and static vessel radius at n_r: $\frac{r_{\text{updated}}}{r_{\text{static}}} < \xi$ for constant $\xi \geq 1$.
(R4) Randomly choose a non-static terminal node n_t of the subtree (FAIL if none is left), shrink the terminal vessel branch at n_t ($r' = 0.9r$), and prune it if $r' \leq 2\,\mu\text{m}$.
(R5) Repeat steps (R1)–(R4) until STOP or FAIL.
(R6) Reinforce static radius at n_r and propagate radii down to subtree terminals [12].

If the tree cannot be remodeled properly (FAIL), we discard the new connection edge and continue with steps (S1)–(S4). Note that we prevent static vessel branches from undergoing any kind of remodeling, degeneration or cropping, except for the adjustment of vessel radii at short isolated branches following the concept of "islands" in [10]. The simulation is ultimately stopped if the surrounding tissue is sufficiently perfused [12].

3 Experiments and Results

We evaluate the performance of the proposed algorithm for TGIF on four synthetic datasets and compare it to different baseline approaches.

Experimental Data. Following the experimental setup of Schneider et al. [12, Fig. 4–6], two artificial arterial tree models are generated for different random seeds. For each of these models we derive a vessel size imaging (VSI) map that is in turn used to synthesize a functionally equivalent but structurally different arterial tree following [5]. The vessel radii range from $(2\text{–}17)\,\mu\text{m}$ in all four cases. We then create artificial gaps by introducing simulated air bubbles (occlusions) at randomly sampled locations within the vessel lumen and cropping the occluded parts of the vasculature. We examine two different configurations for the choice of the size and number of artifacts: In a first set of experiments ($\mathcal{B}_1$), we vary the bubble size $s_{\text{gap}} \in \{3, \ldots, 384\}$[µm], while the number of artifacts is chosen such that the cumulative length of the cropped vessel segments amounts to $\gamma_{\text{crop}} = 5\,\%$ of the total segment length of the ground truth (GT) vasculature. Conversely, in the second configuration ($\mathcal{B}_2$), we consider different crop factors $\gamma_{\text{crop}} \in \{1, \ldots, 32\}[‰]$ for a fixed ensemble of bubble artifacts

($\mathbf{s}_{\text{gap}} = (3, 6, 12, 24, 48, 96)[\mu\text{m}]$). In order to avoid boundary artifacts, we only crop vessel segments within a centered box-shaped region of interest (ROI) (see Figure 1). Likewise, we exclude large vessels ($r > 10\,\mu\text{m}$) that are rarely affected by incomplete filling in real data. From each of the deteriorated vasculatures, we derive an observable counterpart to be used in our infill experiments by modeling the forward imaging and inverse segmentation process as follows: First, we synthesize 3-D image data by sequentially discretizing each vessel segment via a Gaussian point spread function and additive Gaussian noise (isotropic spatial resolution: $1\,\mu\text{m}$). Next, we apply vessel segmentation [11] and skeletonization based on distance-ordered homotopic thinning (DOHT) to reconstruct the vascular structure. Vessel calibers along the skeletonized centerline are determined based on distance transformation. Finally, we apply spline smoothing to each vessel branch and assign a constant radius that preserves the total lumen of the original branch to make the estimation of vessel direction and diameter more robust.

Alternative Methods. On these data we test four alternative gap filling approaches:
(1) Prim's algorithm was applied to extract the *minimum spanning tree (MST)* with each candidate edge connecting a rooted with an unrooted node ($e = (v_r, v_c)$) weighted by the edge length $l(e)$. The radius of candidate edges added to the tree is chosen as the arithmetic mean of the maximum adjacent segment radius at v_r and v_c.
(2) Jiang et al. [2] proposed a different weighting scheme based on Murray's *minimum work principle (MWP)*. The authors derive a simplified cost function for each candidate edge as a mixture of the shortest path tree (SPT) and r^2-weighted MST [2, Eq. 13]:

$$C_{\text{MWP}}\big(e = (v_r, v_c)\big) = \underbrace{l(e) \cdot r^2(e)}_{r^2\text{-MST}} + \underbrace{\lambda_{\text{MWP}} \frac{r_{\text{min}}^3}{2} \cdot \sum_{e_i \in \mathcal{P}(v_c, \hat{v}_r)} l(e_i)/r(e_i)}_{\text{simplified SPT}} \quad , \qquad (2)$$

where $r_{\text{min}} = 2\,\mu\text{m}$ denotes the minimum vessel radius and $\mathcal{P}(v_c, \hat{v}_r)$ the shortest path from candidate node v_c to the closest root node $\hat{v}_r$ of v_r. The radius of candidate edges is chosen as in MST. Following [2], we apply Prim's algorithm for different values of $\lambda_{\text{MWP}} < 1$ (see Table 1) to find the optimal tree minimizing the MWP cost.
(3) The gap filling approach by Risser et al. [10] based on *tensor voting (TV)* was applied as follows: First, we compute the tensor and saliency maps from the vessel network using an isotropic spatial resolution of $1.5\,\mu\text{m}$. For the generation of missing segments we found that the tracking scheme proposed by the authors [10, Eq. 8], i.e., greedily following the maximum saliency in a local neighborhood, can easily fail due to the limited spatial resolution. Thus, we adapt a fiber tracking scheme also used for diffusion tensor imaging to directly track the tensor field rather than the derived saliency measure [6] and use it as a fallback strategy. We perform an exhaustive grid search for each dataset to find the optimal configuration of the four main parameters defining the tensor field and the break criteria during tracking (see Table 1).
(4) Finally, we use the proposed combination of the heuristic cost function in Equation (1) and the k-reciprocal neighborhood scheme in a modified MST-like framework, which can be regarded as a simplified version of TGIF considering topological information only: Unlike standard MST, we consider candidate edges from rooted to unrooted nodes only if they fulfill the k-reciprocal neighborhood condition. We then apply Prim's algorithm to greedily extract the corresponding MST w.r.t. candidate edge weights as defined in Equation (1) for different parameters (see Table 1).

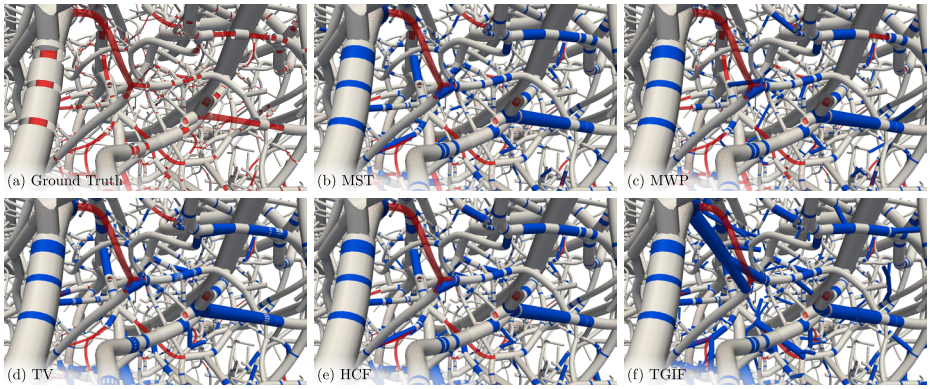

Fig. 2: Close-up views of (a) the ground truth (GT) network in Figure 1 and (b–f) the reconstructed networks generated by different approaches for optimal parameter values minimizing ΔQ_{leaf}. Vessel branches are rendered as cylindrical tubes for the cropped synthetic GT network (gray), cropped gaps (red, radius scaled for better visibility), and reconstructed infill edges (blue).

Our Approach: TGIF. Similar to the baseline experiments, we perform a parameter sweep for selected parameters listed in Table 1. For each parameter set and each input network we run four TGIF simulations using different seeds to account for statistical variations of the reconstructed topologies. As above, the prescribed metabolic profile and angiogenesis parameters are taken from [12].

Quantitative Analysis and Comparison. For the comparison of the different reconstruction approaches we employ four different metrics focusing on different aspects: (1) *Topological correctness* is assessed by a precision-recall analysis. Each infill edge connecting to a static node is counted as true positive if the static target and the proximal interface to the static graph originate from the same bubble artifact (false positive otherwise). False negatives are computed as $(\#\text{gap boundary nodes} - \#\text{true positives} - \#\text{gaps})$. From the derived precision and recall measures, we compute the F_1 score.
(2) As direct comparison of the network topology may not be adequate to capture functional differences, we consider differences in the *path length* from GT nodes v_{GT} to the shortest GT root node $\hat{v}_{\text{GT}}$ [2]: $\Delta E_{\text{path}} = \frac{1}{\|\mathcal{V}_{\text{GT}}\|} \sum_{v_{\text{GT}} \in \mathcal{V}_{\text{GT}}} |l(P(v', \hat{v}')) - l(P(v_{\text{GT}}, \hat{v}_{\text{GT}})|$, where v' is the node of the reconstructed graph that is closest to v_{GT} in an Euclidean sense. As each synthetic arterial tree contains 16 roots in total, the paths may well end up at different roots ($\hat{v}' \ncong \hat{v}_{\text{GT}}$). The path length at unrooted nodes is set to zero.
(3,4) Finally, we compare the *hemodynamic properties* of the reconstructed and GT network. To this end, we simulate the blood flow in the network using pressure boundary conditions at root and leaf nodes where the caliber-dependent pressure values are taken from literature [8]. Terminal nodes of the reconnected networks without any matching leaf node in the GT network are assigned a no-flow boundary condition. From the simulation results, we compute the relative net inflow change at all GT leaf nodes: $\Delta Q_{\text{leaf}} = \sum_{v_{\text{GT}}} \frac{|Q_{\text{in}}(v') - Q_{\text{in}}(v_{\text{GT}})|}{Q_{\text{in}}(v_{\text{GT}})}$. Similarly, we consider the total flow entering the reconstructed and GT network and compare their absolute relative difference ΔQ_{net}.

Close-up views of the reconstructed networks from the different approaches are provided in Figure 2. Topological differences are visually most pronounced for long curved

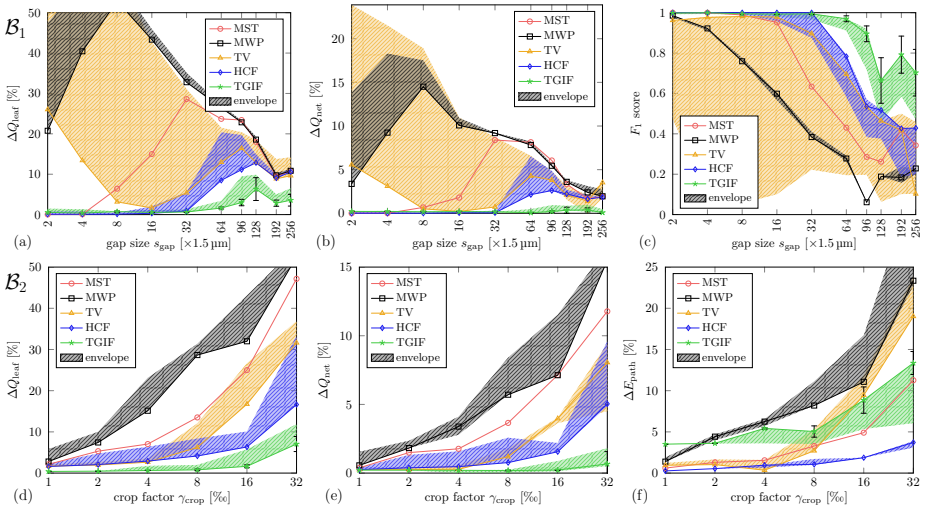

Fig. 3: Quantitative evaluation of different reconnection approaches for varying gap size (a–c) and cumulative artifact length (d–f). (a,d) Relative net inflow change ΔQ_{leaf} at leaf nodes. (b,e) Relative total net inflow change ΔQ_{net}. (c) Topological correctness of infill edges w.r.t. F_1 score. (f) Relative path length error. For each problem size (fixed s_{gap} and γ_{crop}), average values over all four synthetic datasets are marked for each reconnection approach using the optimal parameter configuration (see Table 1) minimizing ΔQ_{leaf}. Shaded areas within each subfigure outline the envelope of the average values obtained by applying these optimal parameters across s_{gap} and γ_{crop}, respectively. Error bars for TGIF indicate the standard deviation across the four datasets.

segments that are difficult to recover. The examples illustrate that TGIF is able to correctly fill most of the gaps and, unlike the other approaches, form bifurcations when necessary. Quantitative results w.r.t. the different metrics are shown in Figure 3 for the different reconnection approaches and both experimental setups ($\mathcal{B}_1$, $\mathcal{B}_2$). In general, the different metrics indicate a decreasing quality of the reconstructed networks for increasing problem size. For increasing gap size ($\mathcal{B}_1$), the topological differences of the GT and reconstructed models become more pronounced as indicated by the decreasing F_1 score. It is remarkable that small changes in topology can have a substantial impact on flow-related errors (see Figures 3a–3c). The figures indicate that TGIF outperforms the baseline approaches. Only for small crop factors, TGIF shows an increased path length error while the flow-related metrics remain consistently small (see Figures 3d–3f). This demonstrates the difficulty of reasonable comparison and validation of vascular networks. The parameter study reveals that, while TV proves to be highly sensitive to the parameter choice, TGIF performs consistently well across different problem sizes and topologies (functionally equivalent but structurally different networks, see above), as indicated by the narrow envelopes and small error bars in Figure 2, respectively. Finally, we find that MST outperforms MWP in our experiments. However, further experiments (not reported here) reveal that, particularly for the synthetic VSI-based networks, Murray's minimum work principle seems to hold at the macroscale only, i.e., excluding the microvasculature ($r \leq 5\,\mu\text{m}$) significantly improves the performance of MWP over MST as reported in [2] for the macrostructure of murine coronary arterial trees.

4 Conclusions and Future Work

We proposed a new method for the reconstruction of complete 3-D arterial trees from partially incomplete image data by combining different key ideas that have been used for the artificial generation of functionally adequate vascular models and different concepts aiming at the correction of vascular connectivity. The experiments demonstrate the effectiveness and superior performance of our approach compared to different state-of-the-art methods for vascular reconstruction. In this work, we have only considered arterial tree models rather than full-fledged vascular networks. Jointly considering arterial and venous networks raises additional problems as recently described in [13]. For instance, vascular remodeling and reconnection have to be reconsidered carefully as the hemodynamics can easily be spoiled by inserting functional shunts. Likewise, it would be interesting to exploit the image data not only for the initial estimation of the (defective) vascular topology but also to further guide and constrain the reconstruction and thus achieve better robustness against inaccuracies in, e.g., vessel direction and caliber.

Acknowledgements. This work has been funded by the Swiss National Center of Competence in Research on Computer Aided and Image Guided Medical Interventions (NCCR Co-Me) supported by the Swiss National Science Foundation.

References

1. Blinder, P. et al.: The cortical angiome: an interconnected vascular network with noncolumnar patterns of blood flow. Nature Neuroscience 16(7), 889–897 (2013)
2. Jiang, Y. et al.: Vessel connectivity using Murray's hypothesis. In: Fichtinger, G., Martel, A., Peters, T. (eds.) MICCAI 2011, LNCS, vol. 6893, pp. 528–536. Springer Heidelberg (2011)
3. Kaufhold, J.P. et al.: Vectorization of optically sectioned brain microvasculature: Learning aids completion of vascular graphs by connecting gaps and deleting open-ended segments. Medical Image Analysis 16(6), 1241–1258 (2012)
4. Lesage, D. et al.: A review of 3D vessel lumen segmentation techniques: models, features and extraction schemes. Medical Image Analysis 13(6), 819–845 (2009)
5. Lloyd, B.A., Hirsch, S., Székely, G.: Optimization of case-specific vascular tree models based on vessel size imaging. In: Bello, F., Cotin, S. (eds.) ISBMS10. LNCS, vol. 5958, pp. 38–48. Springer Berlin/Heidelberg (2010)
6. Mori, S., van Zijl, P.C.M.: Fiber tracking: principles and strategies – a technical review. NMR in Biomedicine 15(7–8), 468–480 (2002)
7. Qin, D. et al.: Hello neighbor: Accurate object retrieval with k-reciprocal nearest neighbors. In: CVPR 2011. pp. 777–784 (2011)
8. Reichold, J.: Cerebral blood flow modeling in realistic cortical microvascular networks. Ph.D. thesis, ETH Zurich, Zurich, Switzerland (2011)
9. Rempfler, M. et al.: Extracting vascular networks under physiological constraints via integer programming. In: MICCAI 2014. LNCS, Springer Berlin/Heidelberg (2014), in press
10. Risser, L., Plouraboue, F., Descombes, X.: Gap filling of 3-D microvascular networks by tensor voting. IEEE Transactions on Medical Imaging 27(5), 674–687 (2008)
11. Schneider, M. et al.: Oblique random forests for 3-D vessel detection using steerable filters and orthogonal subspace filtering. In: Menze, B.H. et al. (eds.) MICCAI-MCV 2012. LNCS, vol. 7766, pp. 142–154. Springer Berlin/Heidelberg (2013)
12. Schneider, M. et al.: Tissue metabolism driven arterial tree generation. Medical Image Analysis 16(7), 1397–1414 (2012)
13. Secomb, T.W. et al.: Angiogenesis: An adaptive dynamic biological patterning problem. PLoS Computational Biology 9(3), e1002983 (2013)

TGIF: Topological Gap In-Fill for Vascular Networks

A Generative Physiological Modeling Approach

– Supplementary Material –

Matthias Schneider[1,2], Sven Hirsch[1], Bruno Weber[2], Gábor Székely[1], and Bjoern H. Menze[1,3]

[1] Computer Vision Laboratory, ETH Zurich, Switzerland
[2] Institute of Pharmacology and Toxicology, University of Zurich, Switzerland
[3] Institute for Advanced Study and Department of Computer Science, TU Munich, Germany

A Heuristic Cost Function

The heuristic cost function (HCF) for an arbitrary candidate edge e connecting a sprouting node v_s with a proximate connection candidate v_c is defined as (see also Equation (1) of the paper):

$$C_{\text{HCF}}(e) = \lambda_{\text{d}} \cdot \frac{l(e)}{d_{\text{max}}} + (1 - \lambda_{\text{d}}) \cdot \left[1 - \exp\left(-\frac{\alpha}{\alpha_0}\right)\right] \left[1 - \operatorname{erf}\left(\frac{l(e)}{d_0}\right)\right] \quad , \quad \text{(A.1)}$$

where $l(e) \leq d_{\text{max}}$ denotes the edge length, and $\lambda_{\text{d}} \in [0, 1]$ is a weighting factor to balance the distance- and angle-based term. The bending angle α is defined as the sum of the bending angles relative to the vessel direction at v_s and v_c, respectively (see Figure A.1). The parameter d_0 defines the maximum distance beyond which the influence of α is negligible. The factor α_0 is used to shape the angle-dependent term. The HCF profile is visualized for different geometric configurations in Figures A.3 and A.2.

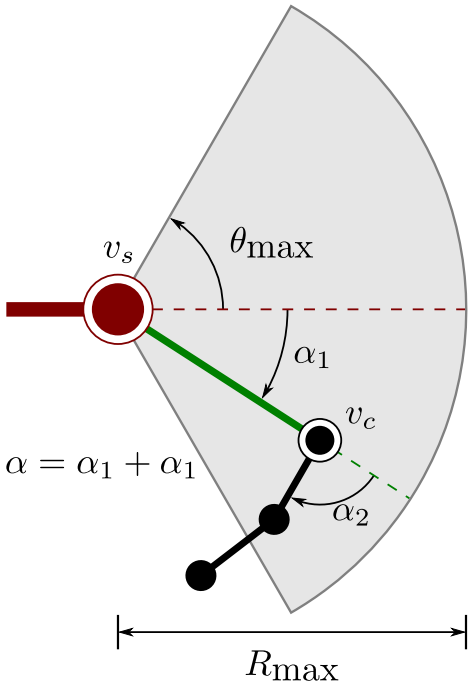

Fig. A.1: Visualization of the reconnection scheme for a 2-D example. The sprouting tip v_s (red) is attracted by (unrooted) vessel segments within in a spherical-cone-shaped sector (gray, maximum distance $R_{\text{max}} = 100\,\mu\text{m}$, angular deviation $\theta_{\text{max}} = 60°$). The bending angle α of the candidate edge (green) linking v_s with candidate node v_c is defined as the sum of the bending angles α_1 and α_2 relative to the vessel direction (dashed) at v_s and v_c, respectively.

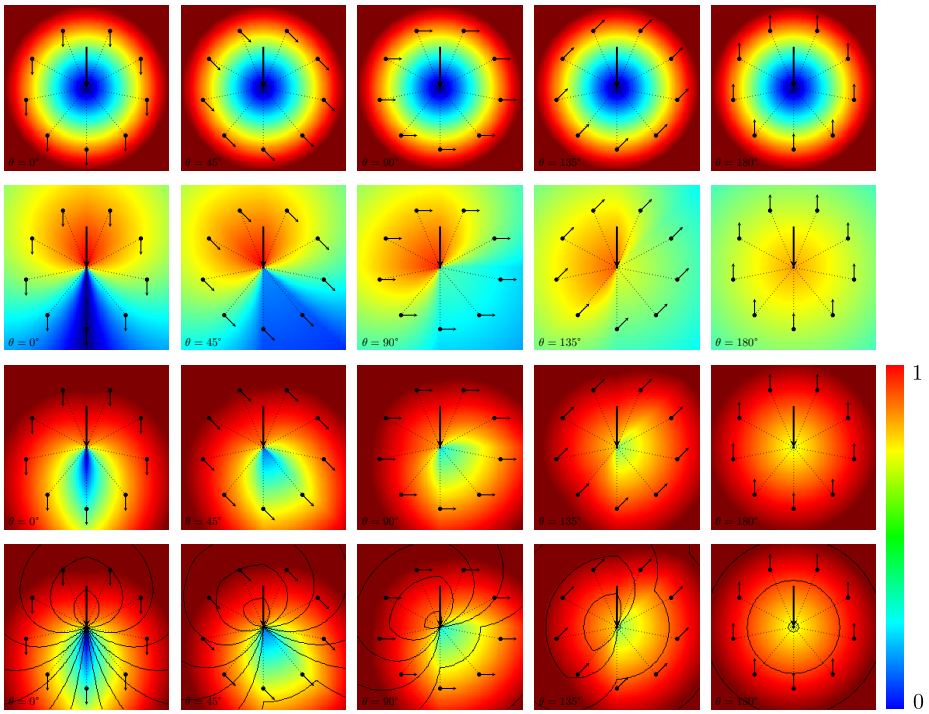

Fig. A.2: Visualization of the heuristic cost function (HCF) used for topological reconnection as defined in Equation (A.1). The parametric model combines a distance- and direction-dependent cost term (first and second row, respectively). The resulting HCF is visualized for different 2-D configurations in the third row and with superimposed isolines of the direction-dependent term in the last row. In each image the large black arrow denotes a vessel segment with the sprouting tip v_s located at the image center. Likewise, small arrows represent the local vessel orientation θ at different connection candidates (black circles) relative to the sprouting tip. The HCF is computed for varying orientation $0 \leq \theta \leq \pi$ (columns) of each candidate edge (dotted lines) using the default parameters provided in Table 1 of the paper ($d_{\text{max}} = 100\,\mu\text{m}$, image dimensions: $200\,\mu\text{m} \times 200\,\mu\text{m}$). Cost function values are color coded. [Best viewed in color.]

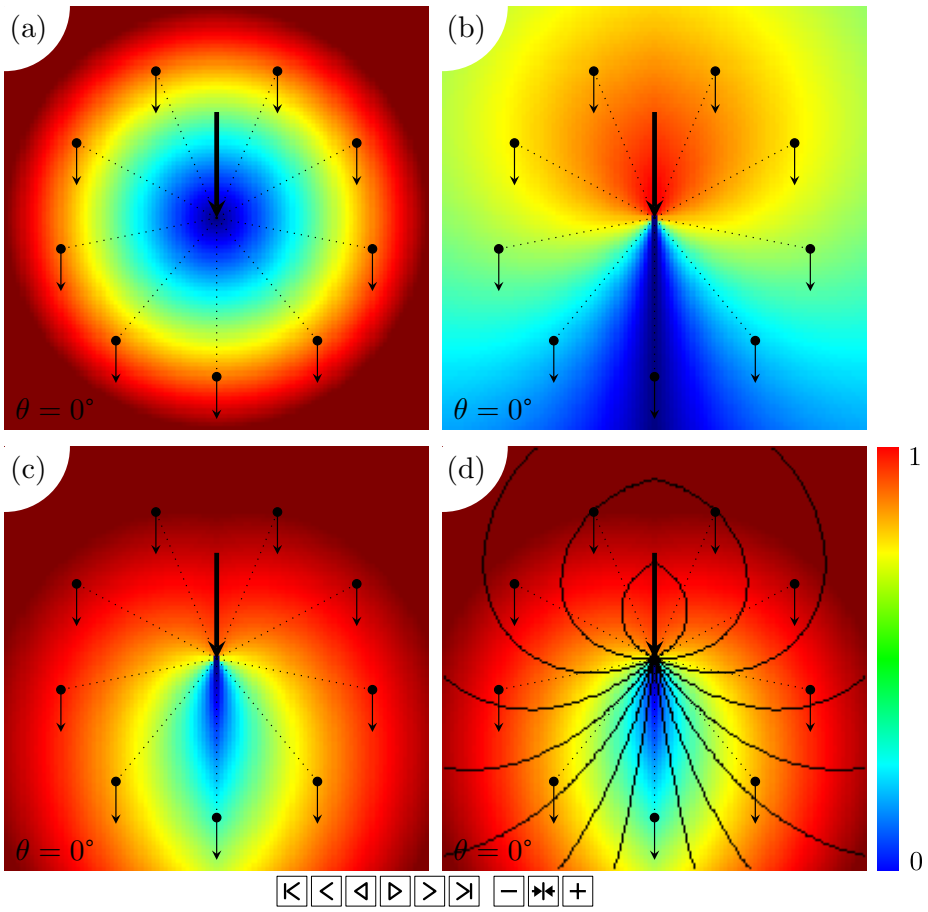

Fig. A.3: Interactive visualization of the heuristic cost function (HCF) used for topological reconnection. (a) Distance-dependent term. (b) Direction-dependent term. (c) Cost function value. (d) Cost function value with superimposed isolines of (b). See caption of Figure A.2 for further details. [Best viewed in color. Animation requires Adobe Acrobat Reader > 7.0]

B Experimental Data and Results

For better visibility, we provide figures with higher resolution for the synthetic vascular tree model (Figure B.1) used in the experiments and the corresponding reconstructed networks obtained from different infill approaches (Figure B.2).

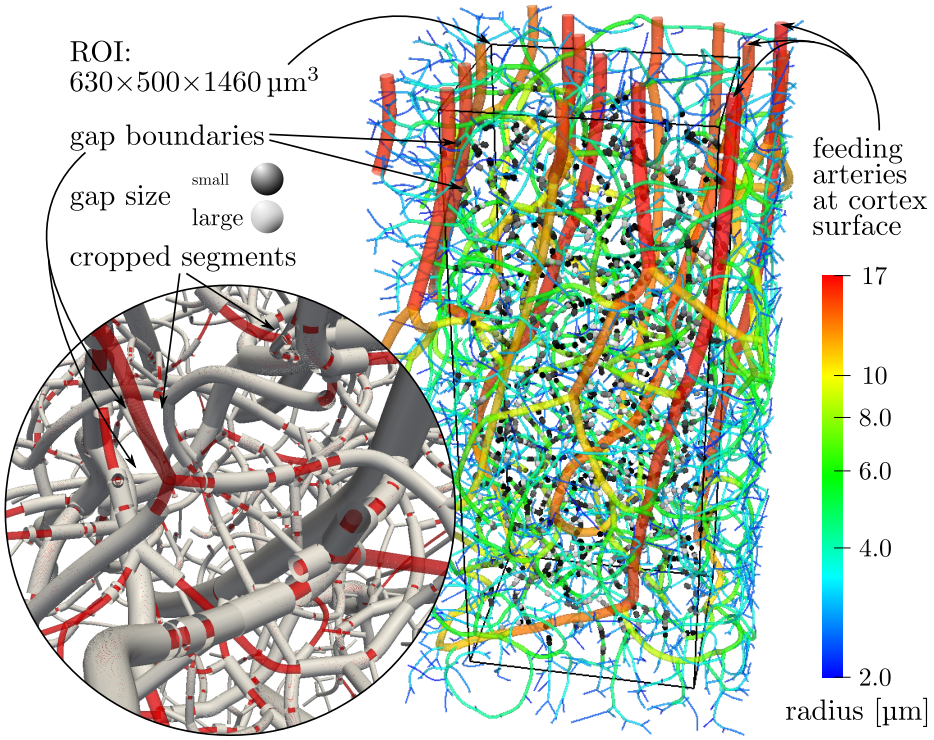

Fig. B.1: Synthetic vascular tree model with artificial gaps ($\mathcal{B}_2$, $\gamma_{\text{crop}} = 32‰$). [Best viewed in color]

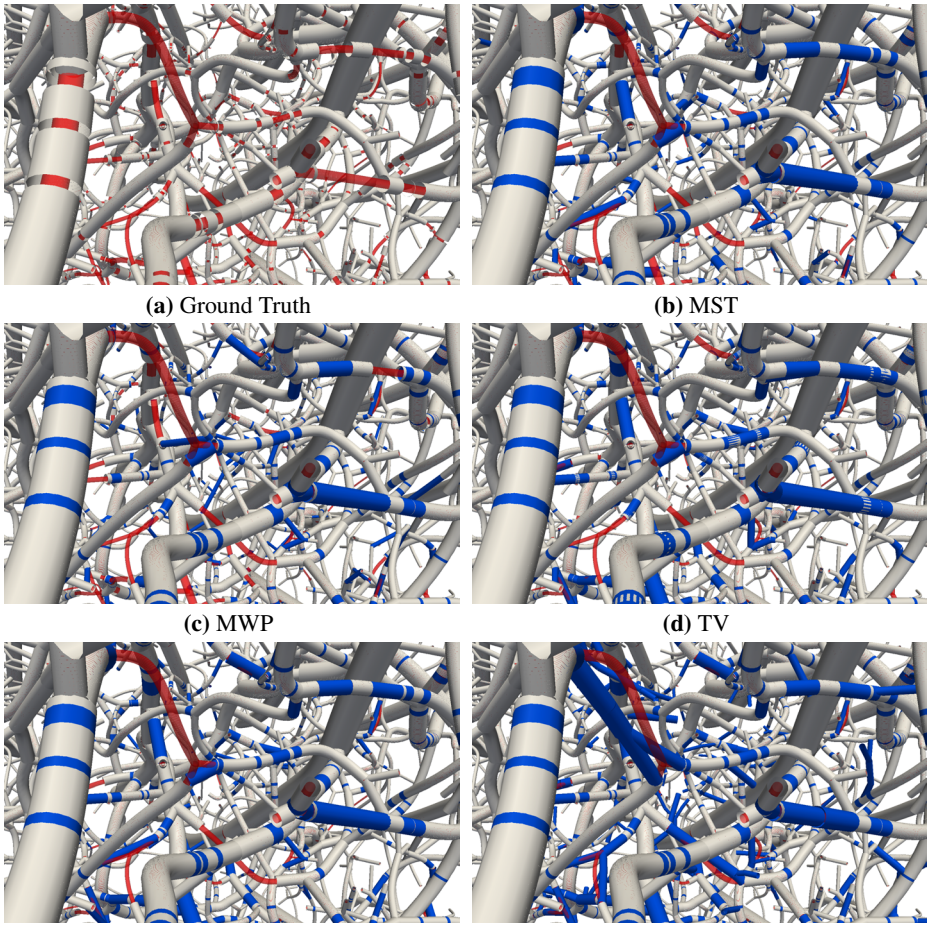

(a) Ground Truth **(b)** MST

(c) MWP **(d)** TV

(e) HCF **(f)** TGIF

Fig. B.2: Closeup views of (a) the ground truth (GT) network in Figure B.1 and (b–f) the reconstructed networks generated by different approaches for optimal parameter values minimizing ΔQ_{leaf}. Vessel branches are rendered as cylindrical tubes for the cropped synthetic GT network (gray), cropped gaps (red, radius scaled for better visibility), and reconstructed infill edges (blue). [Best viewed in color]